ADVANCED MATERIALS
www.advmat.de

Self-Powered Intracellular Drug Delivery by a Biomechanical Energy-Driven Triboelectric Nanogenerator

Zhirong Liu, Jinhui Nie, Bin Miao, Jiadong Li, Yuanbo Cui, Shu Wang, Xiaodi Zhang, Gengrui Zhao, Yongbo Deng, Yihui Wu, Zhou Li, Linlin Li,* and Zhong Lin Wang**

Nondestructive, high-efficiency, and on-demand intracellular drug/biomacromolecule delivery for therapeutic purposes remains a great challenge. Herein, a biomechanical-energy-powered triboelectric nanogenerator (TENG)-driven electroporation system is developed for intracellular drug delivery with high efficiency and minimal cell damage in vitro and in vivo. In the integrated system, a self-powered TENG as a stable voltage pulse source triggers the increase of plasma membrane potential and membrane permeability. Cooperatively, the silicon nanoneedle-array electrode minimizes cellular damage during electroporation via enhancing the localized electrical field at the nanoneedle–cell interface and also decreases plasma membrane fluidity for the enhancement of molecular influx. The integrated system achieves efficient delivery of exogenous materials (small molecules, macromolecules, and siRNA) into different types of cells, including hard-to-transfect primary cells, with delivery efficiency up to 90% and cell viability over 94%. Through simple finger friction or hand slapping of the wearable TENGs, it successfully realizes a transdermal biomolecule delivery with an over threefold depth enhancement in mice. This integrated and self-powered system for active electroporation drug delivery shows great prospect for self-tuning drug delivery and wearable medicine.

Efficient delivery of therapeutics (drugs, proteins, genes, etc.) into desired cells and tissues for both fundamental biological research and therapeutic purposes has vital significance yet presents great challenges.[1] Electroporation uses high-voltage electrical pulses (up to 1000 V) to create transient pores in the plasma membrane for introduction of biologically active molecules into cells.[2] Compared with vesicle/viral vector-assisted delivery, a physical electroporation method has advantages of good repeatability, feasibility for hard-to-transfect cells (e.g., primary cells, stem cells, neurons, immune cells),[3] and preclusion of undesired perturbations.[4] In vitro electroporation has now become a common laboratory transfection method. However, in vivo electroporation drug delivery for therapeutic purposes is still impeded by the lack of applicable, minimally damaging methods that could also obviate patient compliance issues. Moreover, the high voltage during electroporation and its induced heat generation often cause irreparable pores in cell membranes, resulting in irreversible damage to cells and consequent cell death.[5]

Human mechanical motions in daily life, such as limb movement, heartbeats, and respiration, produce abundant kinetic energy.[6] Triboelectric nanogenerator (TENG) could convert these ambient motions into electricity based on the combination of contact

Z. Liu, J. Nie, Dr. S. Wang, X. Zhang, Dr. G. Zhao, Prof. Z. Li, Prof. L. Li, Prof. Z. L. Wang
Chinese Academy of Sciences (CAS) Center for Excellence in Nanoscience
Beijing Institute of Nanoenergy and Nanosystems
Chinese Academy of Sciences
Beijing 100083, P. R. China
E-mail: lilinlin@binn.cas.cn; zhong.wang@mse.gatech.edu

Z. Liu, J. Nie, X. Zhang, Prof. Z. Li, Prof. L. Li, Prof. Z. L. Wang
School of Nanoscience and Technology
University of Chinese Academy of Sciences
Beijing 100049, P. R. China

B. Miao, Prof. J. Li
i-Lab
Suzhou Institute of Nano-Tech and Nano-Bionics
Chinese Academy of Sciences
Suzhou 215125, P. R. China
E-mail: jdli2009@sinano.ac.cn

The ORCID identification number(s) for the author(s) of this article can be found under https://doi.org/10.1002/adma.201807795.

Prof. J. Li, Prof. Y. Deng, Prof. Y. Wu
State Key Laboratory of Applied Optics
Changchun Institute of Optics Fine Mechanics and Physics
Chinese Academy of Sciences
Changchun 130033, P. R. China

Dr. Y. Cui
Stanford University School of Medicine
Palo Alto, CA 94304, USA

Prof. Z. Li, Prof. L. Li, Prof. Z. L. Wang
Center of Nanoenergy Research
School of Physical Science and Technology
Guangxi University
Nanning 530004, P. R. China

Prof. Z. L. Wang
School of Materials Science and Engineering
Georgia Institute of Technology
Atlanta, GA 30332-0245, USA

DOI: 10.1002/adma.201807795

electrification and electrostatic induction.[7] Lightweight, low-cost, and high-stability TENGs have shown great potential in the integration of self-powered systems for energy harvesting and sensing.[8] We speculate that if the biomechanical energy could be harvested via TENG to power in vivo electroporation, it may be a promising way to realize wearable, self-powered, and on-demand drug delivery, solving the problems of poor-compliance and limited tissue accessibility of traditional delivery methods.

We designed a biomechanical energy-driven TENG with the assistance of nanoneedle-array electrode for in vitro and in vivo electroporation drug delivery. Different kinds of TENG structures were fabricated that would be suitable for either in vitro or in vivo electroporation. The electroporation device used for in vitro drug delivery comprises 4 components: i) a portable hand-powered TENG, ii) a rectifier bridge, iii) a 5 × 5 mm silicon nanoneedle-array electrode in the well of a 24-well plate as the anode for cell attachment, and iv) a conventional aluminum (Al) electrode on the cap of the 24-well plate as the cathode (**Figure 1**a and Figure S1, Supporting Information). The hand-powered TENG generates a pulsed electrical field between the cathode and the anode, which passes through each nanoneedle to the cells for electroporation. For in vivo electroporation (Figure 1b), a rectangular freestanding TENG or a contact-separation mode TENG (Figure S2 and Video S1, Supporting Information) is attached on human forearm skin and powered by finger friction or hand slapping. The nanoneedle-array electrode as the anode is attached to the mice skin at the desired location, and a stainless steel needle is embedded under the dorsal skin as the cathode. The integrated, wearable device driven by TENG is intended to achieve transdermal drug delivery and penetration enhancement.

The disk TENG consists of a rotator with a layer of radially arrayed copper (Cu) strips as one frictional layer, a stator with a layer of polytetrafluoroethylene (PTFE) as another frictional material, and a layer of complementary radially arrayed Cu strips as the electrodes (Figure 1c). The output frequency with one hand-cranking revolution in 1 s (rps) can satisfy the needs of electroporation (20 Hz).[9] In the prototype device, to ensure the stability of the output voltage, we used three screws to adjust the relative position between the rotator and stator, which ensured that the two layers were parallel during rotation. Furthermore, we attached a foam layer between the stator and acrylic plate to ensure close contact between the stator and rotator. The open-circuit voltage, short-circuit current, and transferred charge of the disk TENG under 1 rps were about 20 V, 4 μA, and 0.06 μC, respectively (Figure S3a–c, Supporting Information). Through the rectifier bridge, the alternating current pulse of the TENG was successfully transformed into a direct current pulse, and the half-peak width of the pulse was about 25 ms (Figure 1d). The TENG had an extraordinarily high output stability after 30 000 cycles (Figure 1e).

For conventional electroporation, the high voltage and its induced heat generation are the main causes of low cell viability. In the homogeneous electrode field, the pore formation in the cell membrane is a stochastic process. It is impossible to control the electricity so as to match all cells of varying sizes and orientations in one population to form limited and healable electropores.[10] Silicon nanoneedles, as a biocompatible biointerface have been used for electrical sensing,[11] cell force sensing,[12] and delivering species into cells via mechanical penetration.[13] However, intracellular delivery via mechanical penetration alone has low efficiency. We used a silicon nanoneedle array as the electrode for localized electrical field enhancement at the confined nanoneedle–cell interface, which reduced the exerted voltage and its concomitant damage to cells. We fabricated the silicon nanoneedle array using a lithography and a metal-assisted chemical etching process with controllable nanoneedle heights, diameters, and intervals (Figures S5 and S6, Supporting Information). To minimize physical damage to cells,[13,14] we chose an individual nanoneedle with a pointed tip (100 nm in apical width, 700 nm in base diameter, and 7 μm in height) (Figure 1f). The distance between two adjacent nanoneedles was 4 μm, which was roughly 15–50 needles per cell (taking adhered MCF-7 cells as an example). The electrical field simulation showed that at an applied voltage of 20 V, the enhanced electrical field was confined at the tip of each nanoneedle up to ≈2800 V cm^{-1} (Figure 1g). In comparison, a flat silicon electrode and silicon nanoneedle with a cylindrical structure (700 nm in both apical width and base diameter, 7 μm in height) produced only a 200 V cm^{-1} and 458 V cm^{-1} electrical field, respectively (Figure S7, Supporting Information).

We first delivered a small membrane-impermeable molecule of propidiumiodide (PI, Wt = 668.39 Da) by electroporation in MCF-7 human breast cancer cells. After electroporation by hand-cranking disk TENG (1 rps, 10 s, total 200 pulses), PI was successfully delivered into MCF-7 with an efficiency of 85% (**Figure 2**a), similar to a commercial electrical simulator (87%; Figure S9, Supporting Information). In comparison, the delivery efficiencies of cells on the flat electrode with TENG electrical pulses (Flat + TENG) and on the nanoneedle-array electrode without electrical pulses (Needle), were only 9% and 22%, respectively (Figure S9, Supporting Information).

We delivered macromolecular fluorescein isothiocyanate (FITC)-labeled dextran (dextran-FITC, 10 and 70 kDa) using PI as an indicator of dead cells (stained after 24 h of electroporation). The delivery efficiency was about 86% for 10 kDa (Figure 2b) and 49% for 70 kDa dextran-FITC (Figure 2c), respectively (Figures S10 and S11, Supporting Information). The much larger molecular weight and the resulting lower molecule diffusion rate of the dextran (≈70 kDa) compared to PI may explain its relatively decreased delivery efficiency. The cell viability was higher than 94% (Figure 2e), demonstrating that the electroporation system was minimally disruptive.

For genes, physical delivery may solve the poor efficiency limitation of vector-assisted delivery.[15] TENG-enabled electroporation achieved an 82% siRNA delivery (100×10^{-9} M Cy3-labeled siRNA of T-type Ca^{2+} channel protein) into MCF-7 cells, with a cell viability of 94% (Figure 2d–e). After the siRNA delivery, the T-type Ca^{2+} channel protein (Cav3.1) expression was successfully decreased by 71% after another 48 h culture (Figure 2f–h). We further confirmed the versatility of the system in other cell lines, HeLa cells and rat bone mesenchymal stem cells (rBMSCs), a hard-to-transfect primary cell.[14a,16] The delivery efficiencies of dextran-FITC (≈70 kDa) into HeLa and rBMSCs were 63% and 51%, respectively (Figure 2i–j). For all cell lines, the cell viabilities were higher than 94% after electroporation (Figure 2k). After delivery, the dextran-FITC was uniformly distributed in

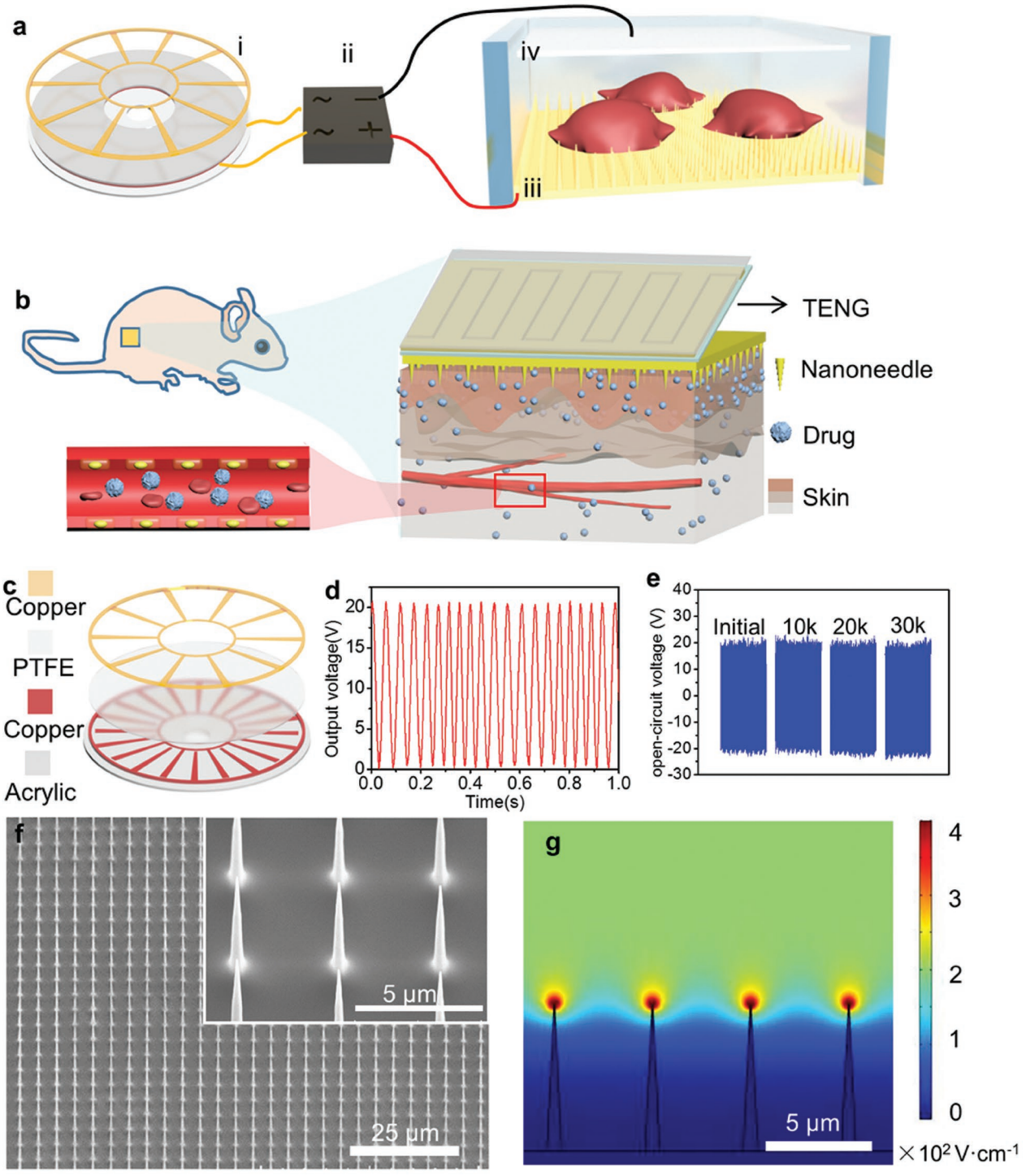

Figure 1. Illustrations of TENG-driven electroporation system. Schematic illustration of a) the in vitro electroporation and b) the in vivo electroporation system. c) Structural design of the disk TENG and its d) output voltage under 1 rps after rectifying, and e) stability of open-circuit voltage over 30 000 cycles. f) SEM images of the silicon nanoneedle array. g) The simulated electrical field distribution of the nanoneedle array at an applied voltage of 20 V.

MCF-7 cells (Figure 2l). Remarkably, there was strong co-localization between the dextran-FITC and the cell nuclei (Figure 2m and Figure S12 and Video S2, Supporting Information), indicating that the exogenous materials were delivered not only into the cytoplasm but also directly into the cell nuclei.

Although high-aspect-ratio nanowire has been proven to be able to penetrate the cell membrane, in our results the delivery efficiency via passive mechanical penetration force alone was low (<23%). With TENG-exerted electrical pulses, the delivery efficiency was enhanced by over four times without

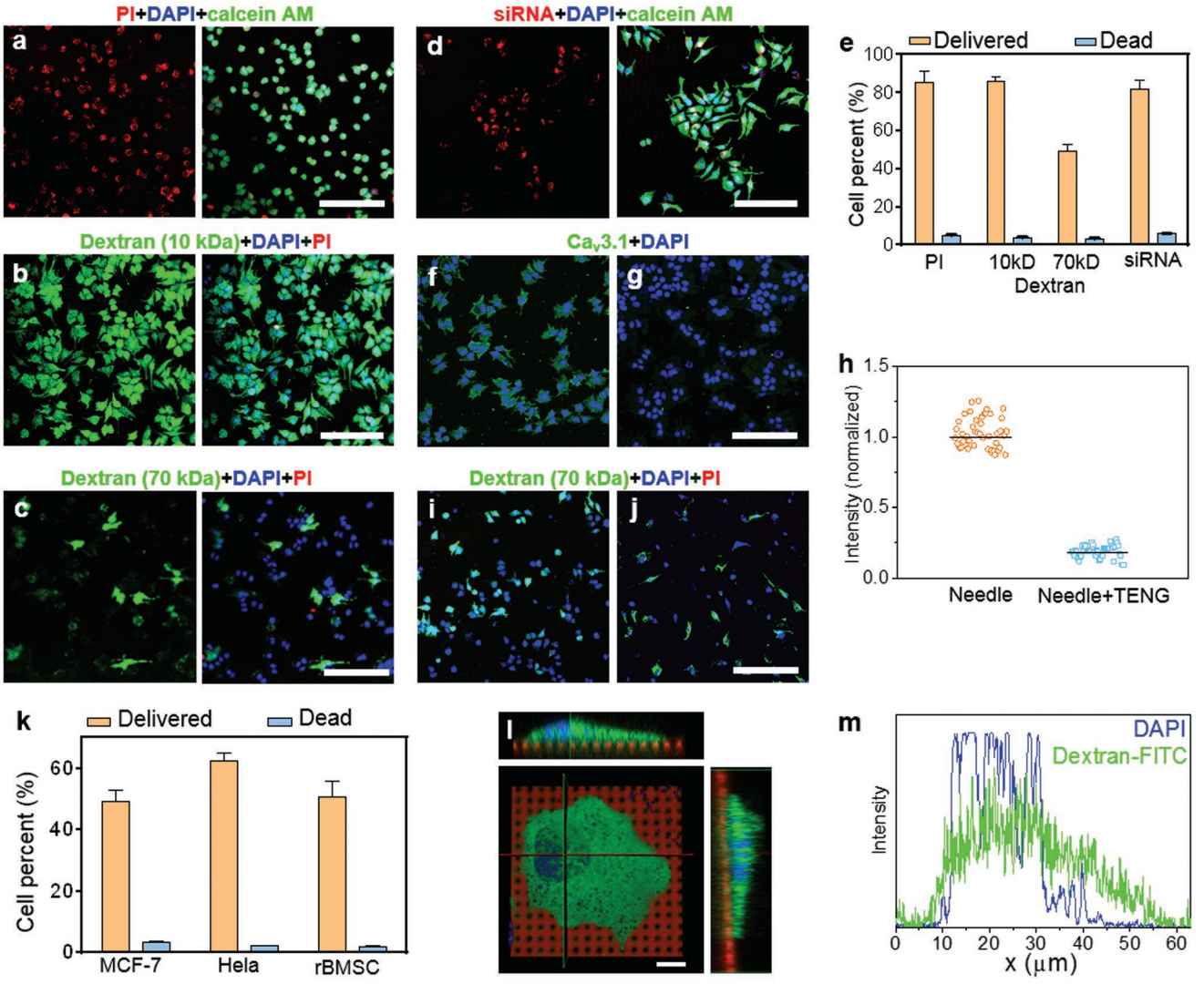

Figure 2. Delivery of diverse biomolecular species into multiple cell types. a) PI delivery into MCF-7. Successfully delivered cells were stained with red PI, and live cells were poststained with green calcein AM. b,c) Dextran-FITC (b: 10 kDa; c: 70 kDa) delivery into MCF-7. Successfully delivered cells were green, and dead cells were poststained with red PI. d) Cy3-siRNA delivery into MCF-7. Successfully delivered cells were stained with red Cy3, and live cells were stained with green calcein AM. e) Quantitative delivery efficiency and cell viability of MCF-7 in a-d. Expression levels of $Ca_v3.1$ protein with another 48 h after f) nanoneedle array and g) nanoneedle array + TENG treatment. h) Quantitative $Ca_v3.1$ expression in f,g). Dextran-FITC (70 kD) delivery into i) HeLa cell and j) rBMSCs. Successfully delivered cells were green, and dead cells were poststained with red PI. k) Quantitative delivery efficiency and cell viability of MCF-7, HeLa, and rBMSCs. l) Fluorescence image of MCF-7 after delivering 70 kDa dextran-FITC (scale bar = 10 μm). The red fluorescence was from autofluorescence of silicon nanoneedle. m) Line scans measured along red line in l. Nuclei were stained with 4′6-diamidino-2-phenylindole (DAPI) in all fluorescent imaging. Error bars, mean ± s.d. Scale bar in a–j, 200 μm.

jeopardizing cell viability. We researched the cell–nanoneedle interaction and electroporation dynamics at the cell–nanoneedle interface. From the focus-ion-beam scanning electron microscopy (FIB-SEM) cross-section images (**Figure 3**a,b), the cell membrane was deformed to engulf the nanoneedle tip. The gap between the cell bottom and the substrate could allow the diffusion of exogenous materials into the cell during electroporation. Silicon nanoneedles were deformed with cellular traction forces in live cells. With the mechanical force, the cell nuclei were also deformed but not pierced by the nanoneedles, as confirmed by the absence of fluorescence at only the middle and lower segments of the nuclei instead of the nuclei top (Figure S13 and Video S3, Supporting Information). Being tightly attached on the nanoneedles, a large number of focal adhesions of the cells were formed at the cell–nanoneedle interface (Figure 3c and Figure S14, Supporting Information).

We monitored the dynamic PI transfer into MCF-7 cells during electroporation. The intracellular PI fluorescence of a total of 17 cells in sight showed that most of the PI molecules were introduced into cells in 80 s, and the molecular entry rate fell down in the next 80 s (Figure 3d and Video S4, Supporting Information). Because the local electrical field enhancement was confined at the nanoneedle tip, we considered that at the nanoneedle–cell interface it would open transient pores during

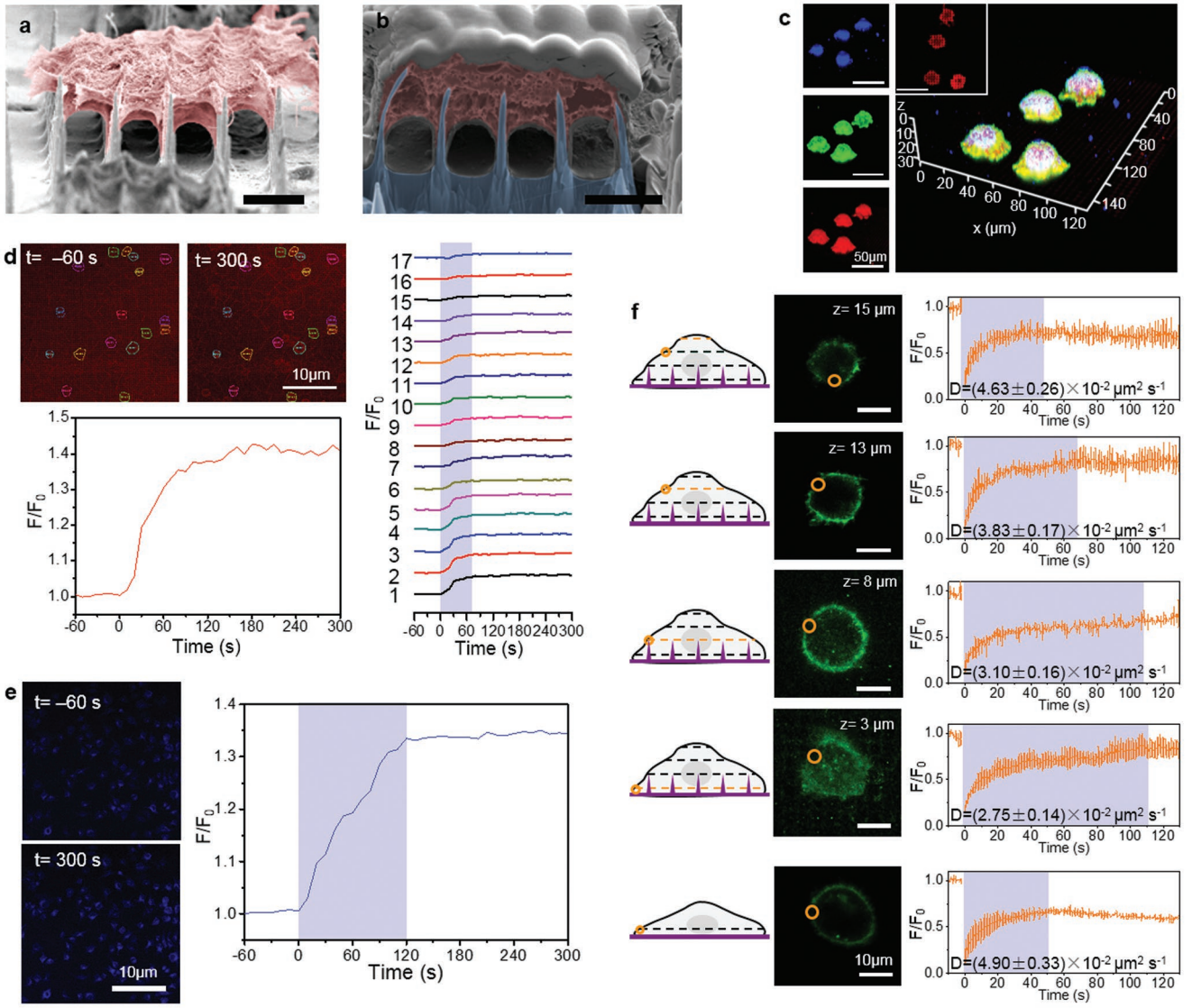

Figure 3. Dynamics at nanoneedle–cell interface. a) SEM and b) FIB-SEM image of MCF-7 on nanoneedle array after seeding for 3 h (scale bar = 5 μm). c) 3D fluorescence morphologies of MCF-7 on the nanoneedle array after seeding for 3 h. Nuclei were stained with blue, F-actin were stained with green, and vinculin was stained with red. Inset shows the vinculin distribution at the middle cross section of the nanoneedles (scale bar = 50 μm). d) PI fluorescence image during electroporation, and the change of PI fluorescence intensity (F/F_0) for all the cells in sight. e) Fluorescence image and normalized fluorescence showing plasma membrane potential during electroporation (scale bar = 10 μm). f) Schematic diagram, fluorescence image, and lipid recovery traces after photobleaching at different cellular heights.

electroporation, followed by membrane resealing after removal of the voltage.[17] The change in plasma membrane potential during electroporation was monitored. After the introduction of electrical pulses, the plasma membrane potential gradually increased over 120 s (Figure 3e and Video S5, Supporting Information), illustrating the enhanced membrane permeability.[18]

The resealing of plasma membrane pores after electroporation is a requisite for cell survival.[19] Membrane resealing is closely related to plasma membrane fluidity, which plays important roles in many biological processes and signaling.[20] Although many researches have focused on the nanowire–cell interface,[21] a fundamental understanding of the influence of nanowire on plasma membrane fluidity is lacking. We monitored the influence of the nanoneedle on plasma membrane fluidity using the fluorescence recovery after photobleaching technique by incorporating 3,3′-dioctadecyloxacarbocyanine perchlorate ($DiOC_{18}(3)$) into plasma membranes (Figure 3f). For cells with 3 h seeding on silicon nanoneedles, membrane fluidity at different cell heights was detected, including the top of the cell that did not adhere to the nanoneedles (z = 15 μm), the middle of the cell that did not adhere to the nanoneedles (z = 13 μm), the middle of the cell that adhered to the tip of the nanoneedles (z = 8 μm), and the bottom of the cell that adhered to the middle of the nanoneedles (z = 3 μm). The diffusion coefficients (D) at the height of 8 μm ($D = 3.10 \times 10^{-2}$ μm^2 s^{-1}) and 3 μm ($D = 2.75 \times 10^{-2}$ μm^2 s^{-1}) was lower than that of 13 μm ($D = 3.83 \times 10^{-2}$ μm^2 s^{-1}) and

15 µm ($D = 4.63 \times 10^{-2}$ µm^2 s^{-1}).[22] At the height of 15 µm, D was close to that of the cells seeded on flat electrode ($D = 4.90 \times 10^{-2}$ µm^2 s^{-1}). This result demonstrated that the fluorescence recovery time was hindered by cell contact with the nanoneedles. We deduced that the nanoneedles mechanically fixed the cell position, reduced membrane fluidity, and prolonged resealing time, which potentially provided additional time for permitting more cargo to enter the cells.

We evaluated the TENG enabled electroporation drug delivery for in vivo transdermal delivery of dextran-FITC (10 kDa; **Figure 4**a and Video S7, Supporting Information). The freestanding TENG (4 × 5.5 cm) attached to a volunteer's forearm skin could be driven by finger friction, achieving an active, self-controlled on-demand drug release (Figure 4b and Video S8, Supporting Information). Alternatively, a contact-separation mode TENG (4 × 4 cm) driven by hand

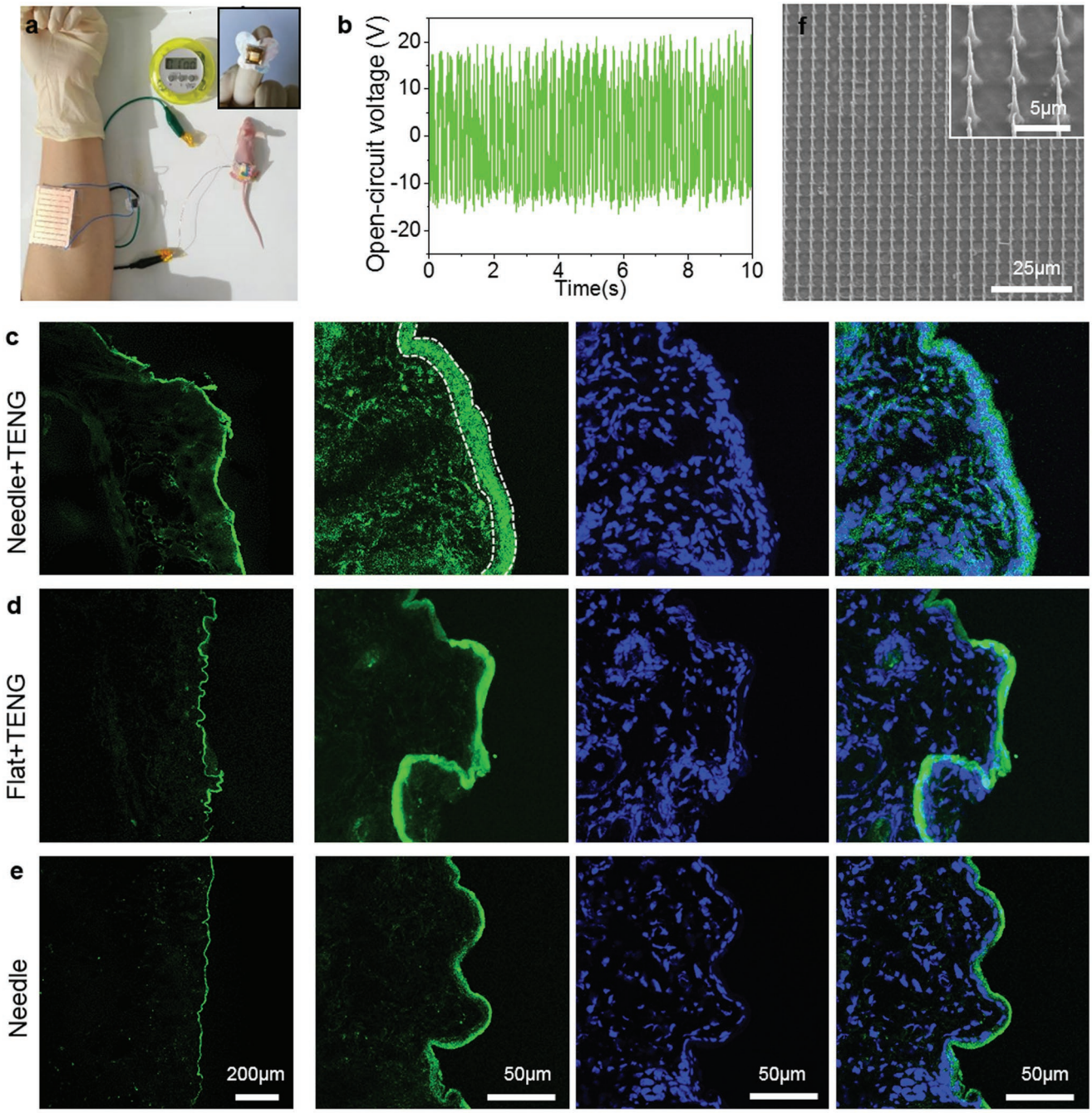

Figure 4. In vivo electroporation drug delivery. a) Photograph of the in vivo electroporation transdermal delivery system. Inset shows the nanoneedle electrode after electroporation with schemochrome. b) Open-circuit voltage of the rectangular freestanding TENG in a) powered by finger friction. Fluorescent images showing tissue sections for 10 kD dextran-FITC delivery after c) nanoneedle array + TENG, d) Flat + TENG, and e) nanoneedle-array treatment. Nuclei were stained with DAPI. f) SEM images of the nanoneedle array after in vivo electroporation.

slapping could also be applicable (Figure S2 and Video S1, Supporting Information). Fluorescent images of tissue cryosections (Figure 4c, Needle + TENG) showed that the dextran-FITC was successfully delivered into dorsal skin of nude mice with a depth of ≈23 µm, higher than that of flat electrode with TENG electrical pulses (11 µm, Figure 4d, Flat + TENG) and nanoneedle-array electrode without electrical pulses (6 µm, Figure 4e, Needle). The drug delivery depth for TENG-powered and nanoneedle-assisted electroporation was far beyond the height of the nanoneedle (over three times), proving the efficient and active penetration of drugs into cells and tissue. Furthermore, it had deeper diffusion depth (light green area in Figure 4c), which may be attributed to the electroporation-enhanced drug diffusion through the rich vascular networks in the dermis. After the in vivo electroporation delivery, the silicon nanoneedle array picked off from the tissue still kept intact structure without breakage (Figure 4f). With a conical structure and tip diameter below 100 nm, the nanoneedle array would cause minimal damage and avoid possible complication of the mice.[23] These results proved the feasibility of using the biomechanical energy-driven TENG for drug delivery in vivo.

TENG as a new era energy technology has been widely used in self-powered and wearable electronics.[24] In this work, by integrating a biomechanical energy-driven TENG with a silicon nanoneedle-array electrode, we achieved noninvasive and high-efficiency electroporation drug delivery in vitro and in vivo. The device is potentially applicable for introducing different kinds of macromolecules into a variety of cell types, including hard-to-transfect primary cells. With a sufficiently high local electrical field in the limited area of the nanoneedle–cell interface, the device had high delivery efficiency and caused minimal cell damage when the voltage was imposed. The self-powered and wearable biomechanical energy-powered TENG enhanced the transdermal delivery of macromolecules into mouse tissue with on-demand delivery, minimal skin irritation and good compliance. We believe that the high-efficiency self-powered electroporation drug delivery system has great potential for future wearable medicine.

Supporting Information

Supporting Information is available from the Wiley Online Library or from the author.

Acknowledgements

Z.L. and J.N. contributed equally to this work. The work was supported by the National Key R & D Project from Minister of Science and Technology (2016YFA0202704), the National Natural Science Foundation of China (No. 81471784, 61573346), the Youth Innovation Promotion Association of the Chinese Academy of Sciences (2015023, 2014278), Nature Science Foundation of Beijing (2172058), and the State Key Laboratory of Applied Optics.

Conflict of Interest

The authors declare no conflict of interest.

Keywords

intracellular delivery, nanoneedle, self-powered, transdermal delivery, triboelectric nanogenerator

Received: December 3, 2018
Revised: January 13, 2019
Published online:

[1] a) D. M. Hallow, R. A. Seeger, P. P. Kamaev, G. R. Prado, M. C. LaPlaca, M. R. Prausnitz, *Biotechnol. Bioeng.* **2008**, *99*, 846; b) C. Chiappini, E. De Rosa, J. O. Martinez, X. Liu, J. Steele, M. M. Stevens, E. Tasciotti, *Nat. Mater.* **2015**, *14*, 532; c) A. Liu, M. Islam, N. Stone, V. Varadarajan, J. Jeong, S. Bowie, P. Qiu, E. K. Waller, A. Alexeev, T. Sulchek, *Mater. Today* **2018**, *21*, 703; d) D. Luo, W. M. Saltzman, *Nat. Biotechnol.* **2000**, *18*, 33.
[2] a) R. Langer, *Nature* **1998**, *392*, 5; b) W. J. Dower, J. F. Miller, C. W. Ragsdale, *Nucleic Acids Res.* **1988**, *16*, 6127.
[3] a) X. Xie, A. Xu, S. Leal-Ortiz, Y. Cao, C. C. Garner, N. A. Melosh, *ACS Nano* **2013**, *7*, 4351; b) D. Schwarz, M. Kollo, C. Bosch, C. Feinauer, I. Whiteley, T. W. Margrie, T. Cutforth, A. T. Schaefer, *Nat. Commun.* **2018**, *9*, 183.
[4] a) R. Gupta, B. Rai, *Langmuir* **2018**, *34*, 5860; b) M. Ouyang, W. Hill, J. H. Lee, S. C. Hur, *Sci. Rep.* **2017**, *7*, 44757.
[5] a) V. Caprettini, A. Cerea, G. Melle, L. Lovato, R. Capozza, J. Huang, F. Tantussi, M. Dipalo, F. De Angelis, *Sci. Rep.* **2017**, *7*, 8524; b) Y. Guo, Y. Zhang, R. Klein, G. M. Nijm, A. V. Sahakian, R. A. Omary, G. Yang, A. C. Larson, *Cancer Res.* **2010**, *70*, 1555.
[6] B. Shi, Z. Li, Y. Fan, *Adv. Mater.* **2018**, *30*, 1801511.
[7] F. Fan, Z. Tian, Z. L. Wang, *Nano Energy* **2012**, *1*, 328.
[8] a) A. Li, Y. Zi, H. Guo, Z. L. Wang, F. M. Fernandez, *Nat. Nanotechnol.* **2017**, *12*, 481; b) W. Guo, X. Zhang, X. Yu, S. Wang, J. Qiu, W. Tang, L. Li, H. Liu, Z. L. Wang, *ACS Nano* **2016**, *10*, 5086; c) P. Song, S. Kuang, N. Panwar, G. Yang, D. J. H. Tng, S. C. Tjin, W. J. Ng, M. B. Majid, G. Zhu, K. T. Yong, Z. L. Wang, *Adv. Mater.* **2017**, *29*, 1605668; d) Y. Jin, J. Seo, J. S. Lee, S. Shin, H.-J. Park, S. Min, E. Cheong, T. Lee, S.-W. Cho, *Adv. Mater.* **2016**, *28*, 7365.
[9] W. Tang, Y. Han, C. Han, C. Gao, X. Cao, Z. L. Wang, *Adv. Mater.* **2015**, *27*, 272.
[10] M. L. Yarmush, A. Golberg, G. Sersa, T. Kotnik, D. Miklavcic, *Annu. Rev. Biomed. Eng.* **2014**, *16*, 295.
[11] J. T. Robinson, M. Jorgolli, A. K. Shalek, M. H. Yoon, R. S. Gertner, H. Park, *Nat. Nanotechnol.* **2012**, *7*, 180.
[12] Z. Li, J. Song, G. Mantini, M. Lu, H. Fang, C. Falconi, L. Chen, Z. L. Wang, *Nano Lett.* **2009**, *9*, 3575.
[13] a) Y. Wang, Y. Yang, L. Yan, S. Y. Kwok, W. Li, Z. Wang, X. Zhu, G. Zhu, W. Zhang, X. Chen, P. Shi, *Nat. Commun.* **2014**, *5*, 4466; b) M. Bok, Y. Lee, D. Park, S. Shin, Z.-J. Zhao, B. Hwang, S. H. Hwang, S. H. Jeon, J.-Y. Jung, S. H. Park, J. Nah, E. Lim, J.-H. Jeong, *Nanoscale* **2018**, *10*, 13502.
[14] C. Chiappini, *ACS Sens.* **2017**, *2*, 1086.
[15] a) D. Bumcrot, M. Manoharan, V. Koteliansky, D. W. Y. Sah, *Nat. Chem. Biol.* **2006**, *2*, 711; b) H. Huang, Z. Wei, Y. Huang, D. Zhao, L. Zheng, T. Cai, M. Wu, W. Wang, X. Ding, Z. Zhou, Q. Du, Z. Li, Z. Liang, *Lab Chip* **2011**, *11*, 163.
[16] M. Zeitelhofer, J. P. Vessey, Y. L. Xie, F. Tubing, S. Thomas, M. Kiebler, R. Dahm, *Nat. Protoc.* **2007**, *2*, 1692.
[17] a) J. Gehl, *Acta Physiol. Scand.* **2003**, *177*, 437; b) S. Somiari, J. Glasspool-Malone, J. J. Drabick, R. A. Gilbert, R. Heller, M. J. Jaroszeski, R. W. Malone, *Mol. Ther.* **2000**, *2*, 178.
[18] a) X. Pan, L. Bai, H. Wang, Q. Wu, H. Wang, S. Liu, B. Xu, X. Shi, H. Liu, *Adv. Mater.* **2018**, *30*, 1800180; b) E. N. Maldonado, J. Patnaik, M. R. Mullins, J. J. Lemasters, *Cancer Res.* **2010**, *70*, 10192.

[19] a) K. Shimizu, H. Nakamura, S. Watano, *Nanoscale* **2016**, *8*, 11897; b) N. W. Andrews, P. E. Almeida, M. Corrotte, *Trends Cell Biol.* **2014**, *24*, 734.

[20] a) S. J. Marrink, A. H. de Vries, D. P. Tieleman, *Biochim. Biophys. Acta, Biomembr.* **2009**, *1788*, 149; b) M. Galic, S. Jeong, F. C. Tsai, L. M. Joubert, Y. I. Wu, K. M. Hahn, Y. Cui, T. Meyer, *Nat. Cell Biol.* **2012**, *14*, 874.

[21] a) A. K. Shalek, J. T. Robinson, E. S. Karp, J. S. Lee, D. R. Ahn, M. H. Yoon, A. Sutton, M. Jorgolli, R. S. Gertner, T. S. Gujral, G. MacBeath, E. G. Yang, H. Park, *Proc. Natl. Acad. Sci. USA* **2010**, *107*, 1870; b) C. Xie, Z. Lin, L. Hanson, Y. Cui, B. Cui, *Nat. Nanotechnol.* **2012**, *7*, 185.

[22] F. Bianchi, L. Syga, G. Moiset, D. Spakman, P. E. Schavemaker, C. M. Punter, A. B. Seinen, A. M. van Oijen, A. Robinson, B. Poolman, *Nat. Commun.* **2018**, *9*, 501.

[23] H. J. Lee, N. Choi, E. S. Yoon, I. J. Cho, *Adv. Drug Delivery Rev.* **2018**, *128*, 132.

[24] a) Z. L. Wang, *ACS Nano* **2013**, *7*, 9533; b) J. Tian, H. Feng, L. Yan, M. Yu, H. Ouyang, H. Li, W. Jiang, Y. Jin, G. Zhu, Z. Li, Z. L. Wang, *Nano Energy* **2017**, *36*, 241.